INTERNATIONAL JOURNAL OF HYDROGEN ENERGY 41 (2016) 14615–14629

Available online at www.sciencedirect.com

ScienceDirect

journal homepage: www.elsevier.com/locate/he

A photoelectrochemical device for water splitting using oligoaniline-crosslinked $[Ru(bpy)_2(bpyCONHArNH_2)]^{+2}$ dye/IrO_2 nanoparticle array on TiO_2 photonic crystal modified electrode

Huseyin Bekir Yildiz [a,*], *Buket Bezgin Carbas* [b,**], *Savas Sonmezoglu* [c], *Mustafa Karaman* [d], *Levent Toppare* [e,f]

[a] *Department of Materials Science and Nanotechnology Engineering, KTO Karatay University, 42020 Konya, Turkey*
[b] *Department of Energy Systems Engineering, Karamanoglu Mehmetbey University, 70100 Karaman, Turkey*
[c] *Department of Metallurgical and Materials Engineering, Karamanoglu Mehmeybey University, 70100 Karaman, Turkey*
[d] *Department of Chemical Engineering, Selcuk University, 42090 Konya, Turkey*
[e] *The Center for Solar Energy Research and Application (GUNAM), Middle East Technical University, 06800 Ankara, Turkey*
[f] *Department of Chemistry, Middle East Technical University, 06800 Ankara, Turkey*

ARTICLE INFO

Article history:
Received 14 April 2016
Received in revised form
27 April 2016
Accepted 28 April 2016
Available online 21 May 2016

Keywords:
Photoelectrochemical cell
Photoanode
Conjugated polymer
Oxidation of water
Metal oxides
Visible light absorbing dyes

ABSTRACT

This article describes the construction of photoelectrochemical cell system splitting water into hydrogen and oxygen using UV–vis light under constant applied voltage. Oligoaniline-crosslinked 2-(4-aminobenzyl)malonic acid functionalized $IrO_2{\cdot}nH_2O$ nanoparticles and visible light absorbing dye, $[Ru(bpy)_2(bpyCONHArNH_2)^{+2}]$ arrays on titanium dioxide (TiO_2) photonic crystals modified electrodes were used as photoanode, and nanostructures based on bonding of Pt nanoparticles by using electropolymerization on poly 4-(2,5-di(thiophene-2-il)-1H-pyrrol-1-il)benzenamine P(SNS-NH_2) conducting polymer modified gold electrode acted as cathode. Each component in anode and cathode of the system was characterized successfully using the methods related. Some optimization studies such as the molar concentration ratio of $[Ru(bpy)_2(bpyCONHArNH_2)^{+2}]$ dye to $IrO_2{\cdot}nH_2O$ nanoparticles, the optimum cycle number of each components and thickness of TiO_2 film were performed in order to investigate the system performance. Furthermore, the photocurrent generation capacity of the photoanode against oxygen resulting and UV stability experiments of photoanode were also investigated. After obtained all necessary informations and improvements of the system, the cell was constructed, and corresponding hydrogen gas evolution from water splitting was calculated as 1.25×10^{-8} mol/cm^2 by using a gas chromatography (GC). The cell generated a photocurrent with a quantum yield of 3.5%.

* *Corresponding author*. Tel.: +90 332 444 1251x7385; fax: +90 332 202 0044.
** *Corresponding author*. Tel.: +90 338 226 2200x5059; fax: +90 338 226 2214.
E-mail addresses: huseyinbekir.yildiz@karatay.edu.tr (H.B. Yildiz), bcarbas@kmu.edu.tr (B.B. Carbas).
http://dx.doi.org/10.1016/j.ijhydene.2016.04.249
0360-3199/

Introduction

Semiconductor-based photocatalytic water splitting using solar irradiation is recognized as one of the ideal approaches to a clean and renewable energy source [1–7]. Photo-electrochemical water splitting was discovered by Fujishima and Honda in 1972 for the first time [8]. In their system, a titanium dioxide (TiO_2) photoanode was exposed to ultraviolet light (UV), producing oxygen and hydrogen at the anode and cathode, respectively. Since then, many groups have attempted to modify this system using visible instead of UV light, and many of these systems share common components [9–12]. A simple way of studying visible light-driven water splitting is to use a dye-sensitized semiconductor oxide material in a photo-electrochemical cell with separate anodic and cathodic compartments to avoid the mixing of H_2 and O_2. Four important components are required to build a light-induced electrochemical system for fuel generation: i) an efficient light-harvesting material with a high molar extinction coefficient (ε) of approximately 90,000 L mol^{-1} cm^{-1} for natural chlorophylls; ii) a molecular donor–acceptor pair for effective charge separation; iii) a robust and efficient water oxidation catalyst; and iv) a transparent conducting electrode surface or a semiconducting material [13–16]. If a semiconductor is used as a light absorber, molecular donor–acceptor pairs are not necessary for charge separation because both light absorption and charge separation are performed by the semiconductor. However, the chemical architecture of a synergetic blend of a water oxidation complex with a light-harvesting unit to trigger high-efficiency photo-electrochemical water oxidation is the major challenge to the use of semiconductors as light absorbers [17]. Similarly, fast charge recombination in most suitable semiconductors occurs much faster than the redox reactions of water, resulting in poor quantum yields [3,18,19]. To meet these challenges, increasing research efforts have now been put into the design and development of new photocatalytic materials (or composites) as well as the novel photocatalytic mechanisms that may lead to further improvement of photoconversion efficiency.

The first example of a functional system for visible-light-driven water oxidation with molecular components was developed by Mallouk and coworkers [20]. In this system, a nanoparticulate anatase TiO_2 surface is sensitized with a heteroleptic ruthenium–polypyridyl chromophore bound through a phosphonate anchor. An IrO_2 nanoparticle catalyst is bound to a ruthenium chromophore through a malonate linkage. The system produces oxygen when illuminated with visible light under a small bias voltage. However, the quantum yield is reportedly 0.9%, and the coulombic efficiency of oxygen production is roughly 20% by Mallouk and coworkers. The relatively poor performance of this system is attributed to a much faster recombination of electrons from the TiO_2 conduction band and the oxidized dye than from the electron transfer between the iridium catalyst and the oxidized dye. Although this system is inefficient, it represents a proof-of-concept that water splitting can be performed using a sensitizer-based photosystem. The low quantum efficiency can be understood in terms of three problems that can be addressed by design at the molecular level. The simplest of these is the needed to make catalyst particles that are connected to only one sensitizer molecule, in order that each sensitizer can bind to both TiO_2 and $IrO_2 \cdot nH_2O$. A second problem is the needed to slow down the back electron transfer reaction, for example, by changing the distance between redox partners, and a third is to speed up the electron transfer from Ir(IV) to Ru(II) [15,21]. To overcome these problems, extensive research efforts are directed toward photo-electrochemical applications of functionalized photoanode/cathode electrodes with novel ligand or anchoring groups and to the design of solar cells, especially because the charge ejection processes lead to low photocurrent yields or even to the elimination of photocurrent. For enhancing the light-electrical energy conversion yield, charge separation of the electron–hole species should be assisted. To this end, coupling relay units to semiconductors associated with electrodes leads to charge separation and enhanced photocurrent generation by trapping the conduction-band electrons in the relay sites and effectively transferring electrons to the electrode. Alternatively, the electrochemical crosslinking of semiconductor nanoparticle monolayers onto electrodes by charge-carrying oligoaniline units has been suggested as a means to facilitate charge separation and to enhance photocurrent generation [22].

In the present study, a photoelectrochemical solar cell was designed using a photoanode with the oligoaniline crosslinked bridging units to serve as both sensitizers ($(Ru(bpy)_2(bpyCONHArNH_2)^{+2}$) and molecular bridges connecting the catalyzer (2-(4-aminobenzyl)malonic acid functionalized $IrO_2 \cdot nH_2O$ nanoparticles) to a metal oxide semiconductor (TiO_2), and using a photocathode including gold electrode coated with Poly(SNS-NH_2) functionalized platinum nanoparticles (Fig. 1). The incorporation of oligoaniline crosslinked bridging units into this device enhances the photocurrent in visible light as well as the quantum yield and efficiency of oxygen/hydrogen production. This is achieved due to strong attachment to the TiO_2 surface, efficient charge separation, and suitable oxidation potential by providing a path for the effective trapping of the conduction-band electrons and their transport to the electrode.

Experimental

Deposition of TiO_2 thin films on PMMA nanofibers by hot filament chemical vapor deposition

Titanium dioxide thin films were deposited conformally over electrospun polymethyl methacrylate (PMMA) fibers using hot filament chemical vapor deposition method. Nanotubular TiO_2 structure was clearly identified via SEM (scanning electron microscope). It was found that this structure was ideal for good photocatalytic activity because of its high surface area per unit volume ratio. FTIR (Fourier Transform Infrared Spectroscopy) and XPS (X-ray Photoelectron Microscopy) results show the formation of stoichiometric TiO_2, and the crystalline form of the final nanotubes was found to be anatase (1 0 1) after XRD analysis. Details deposition procedures of TiO_2 film can be found in our reference [23].

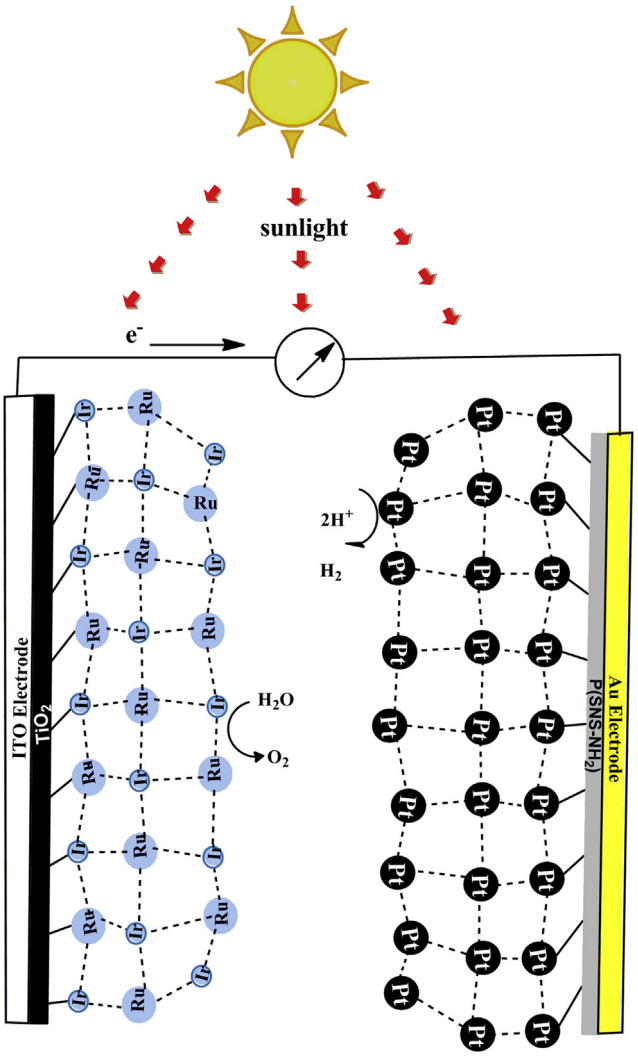

Fig. 1 – Schematic representation of the solar cell to be formed.

Preparation and characterization of photoanode electrode in the photoelectrochemical cell

ITO electrodes modified with TiO_2 was heated overnight in acetonitrile solution containing 3-(4-aminophenyl) propionic acid and so a surface binding formation was occurred between 3-(4-aminophenyl) propionic acid and TiO_2 surface atoms. 3-(4-Aminophenyl) propionic acid-functionalized/TiO_2 film was washed with CH_3CN, toluene and H_2O, respectively. $[Ru(bpy)_2(bpyCONHAr)]^{+2}$ (**6**) and 2-(4-aminobenzyl)malonic acid-conjugated $IrO_2{\cdot}nH_2O$ nanoparticles (**13**) were polymerized in the medium of 0.1 M phosphate buffer solution (pH = 7.4), via cyclic voltammetry (CV) method on 3-(4-aminophenyl)propionic acid-modified TiO_2 film (Fig. 2). For electropolymerization and characterization of this new formation, Pt and saturated calomel electrodes (SCE) were used as counter and reference electrode, respectively. 3-(4-Aminophenyl)propionic acid-modified TiO_2 film was also used as working electrode. It was also queried why both $[Ru(bpy)_2(bpyCONHAr)]^{+2}$ dye and $IrO_2{\cdot}nH_2O$ nanoparticles were used together in the system and the water sensitivity was investigated in comparison with ethanol during oxidation. It was tested whether the cell generates photocurrent. Some optimization studies were also performed. These were the molar ratio between $[Ru(bpy)_2(bpyCONHAr)]^{+2}$ dye and $IrO_2{\cdot}nH_2O$ nanoparticles, the optimum number of cycles of composite formation, the film thickness of TiO_2 coated on ITO electrode. Furthermore, the O_2 formation performance of photoanode was evaluated. For this purpose, Clark-typed electrode system was used to understand how much O_2 gas was produced in water when ITO electrodes modified with $TiO_2/[Ru(bpy)_2(bpyCONHArNH_2)]^{+2}$ dye/$IrO_2{\cdot}nH_2O$ nanoparticle was illuminated for a certain time. For this experiment, ITO electrodes modified with composite and platinum wire were used as working and counter electrodes, respectively, as well as Ag/AgCl electrode as reference electrode under illumination of light at 460 nm.

Synthesis of $[Ru(bpy)_2(bpyCONHAr)]^{+2}$ (6)

Synthetic route of $[Ru(bpy)_2(bpyCONHAr)]^{+2}$ functionalized aniline was shown in Scheme 1. 4,4′-Dimethyl-2,2′-bipyridine (**2**), 2,2′-bipyridine 4,4′-dicarboxylic acid (**3**) and 4,4′-bis-(chlorocarbonyl)-2,2′-bipyridine (**4**) were synthesized according to the literature procedures [24–26]. The syntheses of N^4,N^4-bis(4-aminophenyl)-[2, 2′-bipyridine]-4, 4′-dicarboxyamide (**5**) and bis(2,2′-bipyridine)(4,4′-diphosphonato-2,2′-bipyridine)-ruthenium bromide (**6**) are reported here for the first time.

Synthesis of 4,4′-dimethyl-2,2′-bipyridine (2)

A light yellow solid was obtained in 88% yield. ^{1}H NMR (400 MHz, $CDCl_3$): δ 8.53 (d, J = 4.9 Hz, =CH, 2H), 8.22 (s, =CH, 2H), 7.12 (d, J = 4.9 Hz, =CH, 2H), 2.42 (s, CH_3, 6H). ^{13}C NMR (100 MHz, $CDCl_3$): δ 156.0, 148.9, 148.1, 124.6, 121.9, 21.2.

Synthesis of 2,2′-bipyridine 4,4′-dicarboxylic acid (3)

A white-colored solid was yielded with 90%. ^{1}H NMR (400 MHz, $CDCl_3$): δ 8.53 (d, J = 4.9 Hz, =CH, 2H), 8.22 (s, =CH, 2H), 7.12 (d, J = 4.9 Hz, =CH, 2H), 2.42 (s, CH_3, 6H). ^{13}C NMR (100 MHz, $CDCl_3$): δ 156.0, 148.9, 148.1, 124.6, 121.9, 21.2.

Synthesis of 4,4′-bis-(chlorocarbonyl)-2,2′-bipyridine (4)

The reaction product **4** was used for next reaction.

Synthesis of N^4,N^4-bis(4-aminophenyl)-[2,2′-bipyridine]-4, 4′-dicarboxyamide (5)

4,4′-Bis-(chlorocarbonyl)-2,2′-bipyridine (1.0 g, 3.54 mmol) and p-phenylenediamine (0.76 g, 7.09 mmol) were dissolved in dry THF and than 0.5 mL of triethylamine was added and stirred for 12 h at room temperature. After filtration, solid portions were cleaned with 20 mL of distilled water and 10 mL of diethyl ether. N^4,N^4-bis(4-aminophenyl)-[2, 2′-bipyridine]-4, 4′-dicarboxyamide (1.25 g, 90%) as light green colored powder solid was obtained. ^{1}H NMR (400 MHz, $CDCl_3$): δ 10.33 (s, NH, 2H), 8.89 (d, J = 4.9 Hz, =CH, 2H), 8.86 (s, =CH, 2H), 7.93 (dd, $J_{1,2}$ = 1.5 Hz, $J_{1,3}$ = 4.9 Hz, =CH, 2H), 7.41 (d, J = 8.7 Hz, 4H), 6.56 (d, J = 8.7 Hz, 4H), 5.01 (bs, NH_2, 4H). ^{13}C NMR (100 MHz, $CDCl_3$): δ 159.8, 152.4, 146.9, 142.6, 140.7, 124.4, 119.2, 119.1, 115.39, 1110.6.

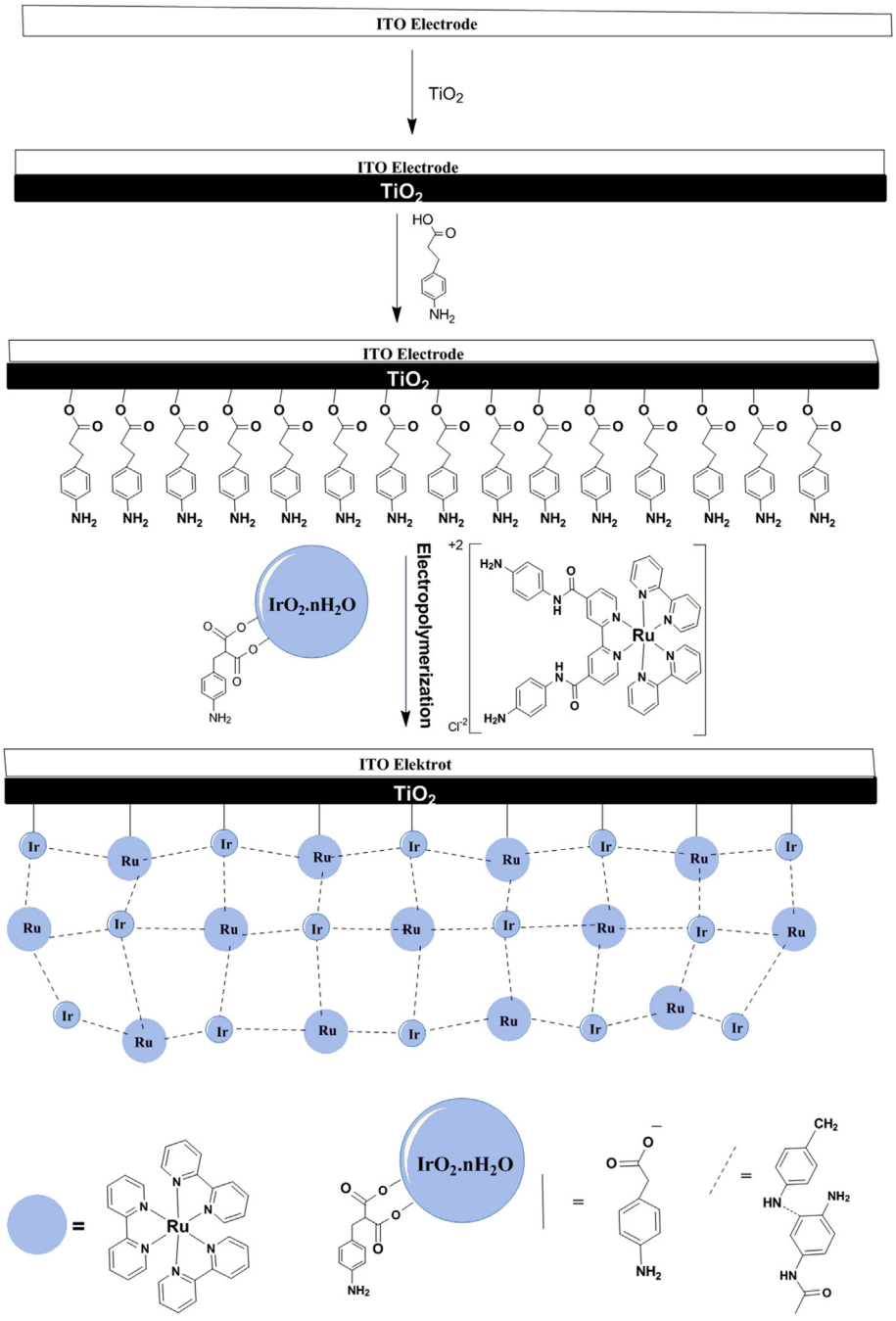

Fig. 2 – Schematic representation of oligoaniline of crosslinking 2-(4-aminobenzyl)malonic acid functionalized $IrO_2{\cdot}nH_2O$ nanoparticles and visible light absorbing dye, $[Ru(bpy)_2(bpyCONHArNH_2)^{+2}]$ on ITO modified with TiO_2.

Synthesis of bis (2,2′-bipyridine)(4,4′-diphosphonato-2,2′-bipyridine)-ruthenium bromide (6)

Cis-Ru (bpy) $2Cl_2{\cdot}2H_2O$ (45 mg, 0.08 mmol) and dicarboxyamide (**5**) (36 mg, 0.08 mmol) were dissolved in 5 mL of EtOH:H_2O (9:1) mixture and it was reflux for 5 h at 100 °C, the solvent was removed in evaporators. The crude product was eluted with Sephadex belt LH-20 in 50% EtOH/CH_3CN solution. The dark red ruthenium complex (60 mg) was obtained in 70% yield. MS-TOF: 871.3209 $[M - HCl]^+$. ^1H NMR (400 MHz, CD_3CN): δ 9.99 (s, NH, 2H), 9.42 (s, =CH, 2H), 8.49–8.45 (m, =CH, 4H), 8.33 (d, J = 6.0 Hz, =CH, 4H), 8.21–8.10 (s, =CH, 6H), 7.83–7.73 (m, =CH, 4H), 7.60–7.58 (m, =CH, 2H), 7.18–7.135 (m, =CH, 4H). ^{13}C NMR (100 MHz, d-CD_3CN): δ 157.94, 153.31, 153.02, 152.96, 151.68, 137.31, 136.84, 136.28, 136.16, 135.84, 126.61, 126.54, 126.04, 125.3, 124.93, 123.21, 123.18, 13.09, 122.89.

Synthesis of $IrO_2{\cdot}nH_2O$ nanoparticles functionalized 2-(4-amino-benzyl)malonic acid

2-(4-Amino-benzyl)malonic acid was synthesized by following the synthesis steps as shown in Scheme 2.

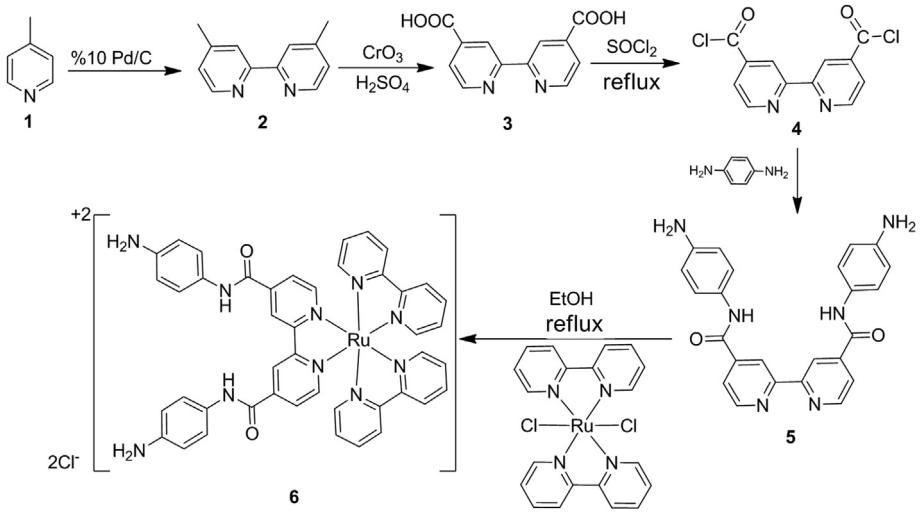

Scheme 1 – Synthetic route for $[Ru(bpy)_2(bpyCONHArNH_2)]^{+2}$ functionalized with aniline.

$IrO_2 \cdot nH_2O$ nanoparticles functionalized 2-(4-amino-benzyl) malonic acid was prepared by using different ratios between $IrO_2 \cdot nH_2O$ and 2-(4-amino-benzyl)malonic acid molecules.

Synthesis of synthetic material dimethyl 2-(4-nitrobenzylidene) malonate (9) [27]

Yellow crystals were obtained in 86% yield. ^{1}H NMR (400 MHz, CDCl3): δ 8.25 (d, J = 7.0 Hz, =CH, 2H), 7.81(s, =CH, 1H), 7.43(d, J = 7.0 Hz, =CH, 2H), 3.89 (s, $-OCH_3$, 3H), 3.85 (s, $-OCH_3$, 3H).

Synthesis of dimethyl 2-(4-nitrobenzyl) malonate (10)

Dimethyl 2-(4-nitrobenzylidene)malonate (0.5 g, 1.89 mmol) (9) were dissolved in 8 mL of methanol and $NaBH_3CN$ (0.47 g, 7.5 mmol) was added onto the mixture over 5 min, stirred at room temperature for 16 h 9 mL of pure water was added to the mixture and pH of the solution was adjusted to 2.5 with HCl. The solution was made work-up with (3 × 30 mL) $CHCl_3$. After the organic phase was dried with Na_2SO_4 and the solvent was removed in evaporator, the crude product was obtained as a yellow fluffy solid (486 mg, 95% yield). ^{1}H NMR (400 MHz, $CDCl_3$): δ 8.16 (d, J = 8.8 Hz, =CH, 2H), 7.39 (d, J = 8.8 Hz, =CH, 2H), 3.72 (s, $-OCH_3$, 6H), 3.70 (t, J = 7.8 Hz, CH, 1H), 3.33 (d, J = 7.8 Hz, CH_2, 2H).

Synthesis of dimethyl 2-(4-aminobenzyl)malonate (11)

10% Pd/C (0.31 g) was carefully added into 5 mL dry methanol. It was dissolved in 50 mL dry methanol solution and added into dimethyl 2-(4-nitrobenzyl)malonate (3.16 g, 11.9 mmol)

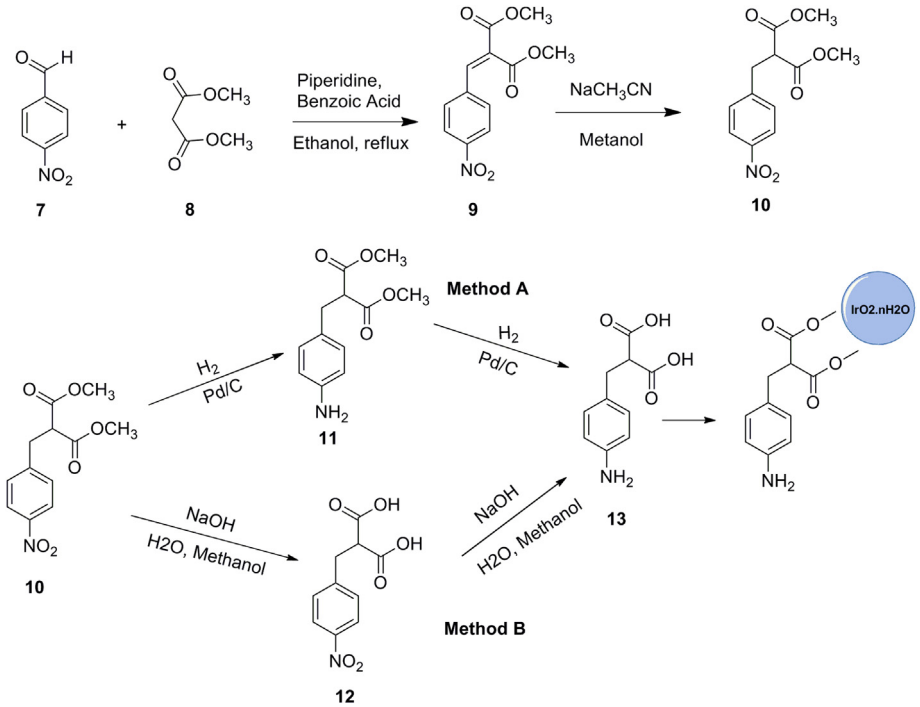

Scheme 2 – Synthetic route of 2-(4-amino-benzyl)malonic acid functionalized $IrO_2 \cdot nH_2O$ nanoparticles.

(**10**) and Pd/C methanol solution. The reaction mixture was subjected to hydrogenation at room temperature under a hydrogen atmosphere. At the end of the reaction, Pd/C was separated from the solution by filtration. The solvent was removed in vacuum and a brown colored oily dimethyl 2-(4-aminobenzyl)malonate (2.48 g, 88%) was obtained. ^{1}H NMR (400 MHz, $CDCl_3$): δ 6.97 (d, $J = 8.4$ Hz, CH, 2H), 6.60 (d, $J = 8.4$ Hz, CH, 2H), 3.69 (s, 2× OCH_3, 6H), 3.60 (t, $J = 8.0$ Hz, CH, 1H), 3.10 (d, $J = 8.0$ Hz, CH_2, 2H). ^{13}C NMR (100 MHz, $CDCl_3$): δ 169.40, 145.07, 129.67, 127.60, 115.29, 54.02, 52.49, 34.08.

Synthesis of dimethyl 2-(4-nitrobenzyl)malonic acid (12)
Dimethyl 2-(4-nitrobenzyl) malonate (1.33 g, 5 mmol) was dissolved in 20 mL of methanol. A solution of NaOH dissolved in 10 mL of deionized water (0.44 g, 22:32 mmol) was added onto the solution and stirred for 3 h at 55 °C. pH of the mixture at room temperature were found 9 with a pH meter paper. pH was adjusted to approximately 3 with HCl. Yellowish crystals were obtained from the solution. The crystals were dried under vacuum of 2-(4-nitrobenzyl)malonic acid (0.714 g, 60%) was obtained. ^{1}H NMR (400 MHz, *d*-DMSO): δ 12.90–12.80 (brs, −COOH, 2H), 8.13 (d, $J = 8.8$ Hz, =CH, 2H), 7.52 (d, $J = 8.8$ Hz, =CH, 2H), 3.69 (t, $J = 7.9$ Hz, CH, 1H), 3.15 (d, $J = 7.8$ Hz, CH_2, 2H).

Synthesis of 2-(4-aminobenzyl)malonic acid (13)
Method A. 2-(4-Nitrobenzyl)malonic acid (2.39 g, 10 mmol) was dissolved in 20 mL of dry methanol and 10% Pd/C (0.60 g) was added. The reaction mixture was stirred in a hydrogen atmosphere at room temperature for 18 h. At the end of the reaction, the crude product Pd/C was removed by filtration. The solvent was removed from the solution in vacuum and the crude product was crystallized with EtOH/hexane solution. Orange-colored crystals (1.67 g, 80%) was obtained. ^{1}H NMR (400 MHz, *d*-DMSO): δ 12.90–12.80 (bs, −COOH, 2H), 8.13 (d, $J = 8.8$ Hz, CH, 2H), 7.52 (d, $J = 8.8$ Hz, CH, 2H), 3.69 (t, $J = 7.9$ Hz, CH, 1H), 3.15 (d, $J = 7.8$ Hz, CH_2, 2H).

Method B. Dimethyl 2-(4-aminobenzyl)malonate (2.37 g, 10 mmol) was dissolved in 30 mL of methanol. A solution of NaOH dissolved in 15 mL of deionized water (0.66 g, 33.48 mmol) was added onto the solution and stirred for 3 h at 55 °C. pH of the mixture at room temperature were found 9 with pH meter paper. pH was adjusted to approximately 3 with HCl. Orange colored crystals were obtained from the solution. The crystals were dried under vacuum of 2-(4-aminobenzyl)malonic acid (1.4 g, 70%) was obtained. ^{1}H NMR (400 MHz, *d*-DMSO): δ 10.27–10.17 (bs, −COOH, 2H), 7.34 (d, $J = 8.4$ Hz, CH, 2H), 7.27 (d, $J = 8.4$ Hz, CH, 2H), 4.2–4.1 (bs, NH_2, 2H), 3.59 (t, $J = 7.8$ Hz, CH, 1H), 3.02 (d, $J = 7.9$ Hz, CH_2, 2H). ^{13}C NMR (100 MHz, *d*-DMSO): δ 170.02, 138.48, 130.12, 129.65, 123.03, 53.16, 33.59.

Synthesis of 2-(4-amino-benzyl)malonic acid functionalized $IrO_2{\cdot}nH_2O$ nanoparticles
A molar [2-(4-aminobenzyl)malonic acid]/[Ir] ratio to be 100/1, K_2IrCl_6, 2-(4-aminobenzyl)malonic acid (38 mL) was placed into a 100 mL flask. After the pH of this aqueous solution was adjusted to 7.5, it was heated at 90 °C for 30 min. The pH of the medium was again adjusted to 7.5 after being cooled in an ice bath taken from heater. The mixture was refluxing for 2 h and air was given to the mixture. The mixture was cooled to room temperature after heating. After reaching room temperature, the mixture was filtered using cotton balls and then chromatographed on Sephadex LH-20 using water as the developing solvent. The first band, dark brown was diluted to 20 mL and collected to give a purple product.

Preparation and characterization of cathode electrode in the photoelectrochemical cell

$SNS\text{-}NH_2$ monomer was electropolymerized in the medium of sodium perchlorate ($NaClO_4$) lithium perchlorate ($LiClO_4$) and acetonitrile (ACN) solvent electrolyte couple on the surface of gold electrode by using cyclic voltammetry method. And then Pt nanoparticles functionalized with the mercaptoaniline was electropolymerized in the medium of 0.1 M phosphate buffer (pH = 7.4) over conjugated polymer P($SNS\text{-}NH_2$) electropolymerized on Au electrode (1 cm^2) beforehand and so crosslinked oligoaniline formation between two layer was occurred. The cycle numbers of conductive polymer was optimized when the cycle numbers of Pt nanoparticles (1 mg/mL) were constant (100 cycles) during electropolymerization in the medium of 0.1 M phosphate buffer solution (pH = 7.4). The cycle numbers of Pt nanoparticles were also optimized by keeping constant optimized cycle number of P($SNS\text{-}NH_2$) formation in previous step. After the cathode electrode was formed, its reduction performance was tested by 9 mM hydrogen peroxide (H_2O_2) solution in 0.1 M phosphate buffer solution (pH = 7.4), to get best results from the solar cell experiments.

Preparation of platinum nanoparticles functionalized with the mercaptoaniline
The three separate solutions were used in the synthesis of nanoparticles. Number one solution was prepared by dissolving 300 mg of $PtCl_4$ in 75 mL of hexylamine. The solution volume of number two was prepared by dissolving tiyoaniline (35 mg, 0.28 mmol) sodium salt of 2-mercapto ethane sulfonic acid (180 mg, 0.11 mmol) in a volume of the solution of 30 mL of methanol/hexylamine (1/1). The number three with a volume of solution 40 mL water/methanol mixture (1/1) was prepared by adding 300 mg of sodium borohydride. After stirring the solution at room temperature, number three in number vigorously mixture was turned to brown color of the solution within a few seconds and added to solution number two brown mixture after 1 min. After 3 min, 200 mL of pure water was added to this new mixture and stirred for 15 min. Then the mixture was transferred to a separating funnel to remove the water phase medium. The organic phase was washed repeatedly with 200 mL water solution. The volume of the organic phase at 35 °C was reduced to 3–4 mL with a rotary evaporator system. In the next step, tiyoaniline (35 mg, 0.28 mmol) and sodium salt of 2-mercapto ethane sulfonic acid (180 mg, 0.11 mmol) was dissolved in 15 mL of ethanol and was added to the organic phase. The latest resulting mixture was stirred overnight. The black residue passed through a centrifuge machines several times and were collected then washed 3–4 times with diethyl ether. Pt has been estimated to be prepared nanoparticle size of 4–5 nm in diameter.

Synthesis of 4-(2,5-di (thiophen-2-yl)-1H-pyrrol-1-yl) benzenamine (SNS-NH_2) monomer

In the literature [28,29] as indicated, our reagent was 1,4-di (2-thienyl)-1,4-butanedione agent thiophene and succinyl chloride, aluminum chloride ($AlCl_3$) catalyzed by use of the Friedel–Crafts reaction was synthesized. Then 1,4-di (2-thienyl)-1,4-butanedione with benzene-1,4-diamine in the solution of toluene catalyzed with propionic acid was reacted and 4-(2,5-di (thiophene-2-yl)-1-H-pyrrol-1-yl)benzenamine (SNS-NH_2) was synthesized. ^{1}H NMR (400 MHz, $CDCl_3$) (δ/ppm): 7.76 ppm (d, 2H), 7.59 ppm (d, 2H), 7.08 (t, 2H), 3.33 ppm (t, 4H). ^{13}C NMR (100 MHz, $CDCl_3$) (δ/ppm): 191.6 ppm (CO), 143.6, 133.6, 132.1, 128.0, 32.7 ppm.

Water splitting experiments under visible light

In the experiments of water splitting under visible light, nanostructure, which was formed by bonding conductive crosslinked oligoanilines bridges of Ru(bpy)$_2$(bpy-CONHArNH$_2$)$^{+2}$dye and $IrO_2{\cdot}nH_2O$ nanoparticles over ITO electrode modified with TiO_2 photonic crystals was used as photoanode. The structure, which was formed by bonding of electropolymerized Pt nanoparticles on the surface of gold electrode modified with P(SNS-NH_2) was used as cathode 1.5–2.0 mm distance away photoanode. The cathode and anode electrodes were connected in series to potentiostat device with a 1 kΩ resistance and were also connected to a multimeter to measure the voltage across the resistance of the resistor. In this system, voltage readings from the multimeter Pt nanoparticles/P(SNS-NH_2) have shown that electron currents towards the gold electrode modified with the polymer. This electron flow will be evidence of the oxygen produced in the anode section. The H_2 gas produced by the cathode was determined via gas chromatography method by getting gas sample with a microsyringe from the system (Fig. 1).

Result and discussion

Fabrication of photo-anode electrode for solar cell

Synthesis and characterization of [Ru(bpy)$_2$(bpyCONHAr)]$^{+2}$ dye modified aniline and $IrO_2{\cdot}nH_2O$ nanoparticles functionalized 2-(4-aminobenzyl)malonic acid

To obtain desired photo-anode electrode site for our solar cell system (Fig. 2), the starting materials 4,4′-dimethyl-2,2′-bipyridine (**2**), 2,2′-bipyridine 4,4′-dicarboxylic acid (**3**), 4,4′-bis-(chlorocarbonyl)-2,2′-bipyridine (**4**), N^4,N^4-bis(4-aminophenyl)-[2,2′-bipyridine]-4, 4′-dicarboxyamide (**5**), were successfully synthesized and characterized with common chemical characterization methods for synthesis of [Ru(bpy)$_2$(bpyCONHAr)]$^{+2}$ (**6**). ^{1}H NMR, ^{13}C NMR and MS-TOF data were given in supplementary. Since the solubility of Ruthenium complex was very low, the resolution of proton NMR was not so good (Fig. S1a) and Carbon NMR samples were kept in the system for too long to see the peaks for characterization (Fig. S1b). The mass of the molecule is taken to ensure full characterization of the molecule (Fig. S1c) 2-(4-aminobenzyl)malonic acid (**13**), dimethyl 2-(4-nitrobenzyl) malonic acid (**12**), 2-(4-aminobenzyl) malonate (**11**), dimethyl 2-(4-nitrobenzyl) malonate (**10**), dimethyl 2-(4-nitrobenzylidene) malonate (**9**), were synthesized and then used as starting materials to synthesize $IrO_2{\cdot}nH_2O$ nanoparticles functionalized with 2-(4-aminobenzyl)malonic acid.

[2-(4-aminobenzyl)malonic acid]/[Ir] were optimized by preparing different ratios (1/1, 10/1 and 100/1) for the synthesis of $IrO_2{\cdot}nH_2O$ nanoparticles functionalized 2-(4-aminobenzyl)malonic acid with 2 nm in diameter. It was observed that the aggregations were formed via transmission electron microscopy when IrO_2 nanoparticles were synthesized using the ratio of 1/1 and 10/1. In the case of 100/1 ratio, these aggregations were disappeared and nanoparticles with 2 nm in diameter were successfully synthesized (Fig. 3).

The electropolymerization of [Ru(bpy)$_2$(bpyCONHAr)]$^{+2}$ modified aniline and $IrO_2{\cdot}nH_2O$ nanoparticles functionalized 2-(4-aminobenzyl)malonic acid was performed in the presence of 0.1 M phosphate buffer solution (pH = 7.4) by cyclic voltammetry in the potential range of −0.4 V and +0.4 V on 3-(4-aminophenyl) propionic acid-functionalized/TiO_2 film as working electrode under Argon atmosphere. In order to ensure about the crosslinked oligoaniline formation, electropolymerized film was also characterized in the medium of 0.1 M phosphate solution (pH = 7.4). As seen in Fig. 4 and its inset the redox couple indicates the formation of crosslinked-oligoaniline and the oxidation potentials of crosslinked-oligoaniline in different pH values, respectively.

Photocurrent generation experiments of ITO electrode modified with TiO_2/[Ru(bpy)$_2$(bpyCONHArNH$_2$)]$^{+2}$ dye/$IrO_2{\cdot}nH_2O$ nanoparticles structure

Some of control experiments were carried out to understand how photocurrent was occurred by ITO electrode modified with TiO_2/[Ru(bpy)$_2$(bpyCONHAr)]$^{+2}$ dye/$IrO_2{\cdot}nH_2O$ nanoparticle structure after fabrication of photoanode electrode as

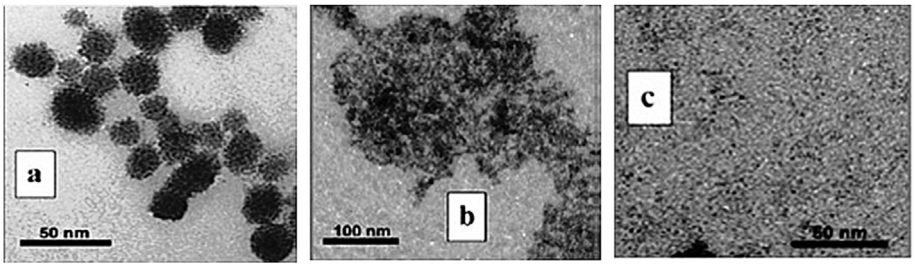

Fig. 3 – TEM morphologies of [2-(4-aminobenzyl)malonic acid]/[Ir] ratio of a) 1.1, b) 1.10 and c) 100/1 to be synthesized $IrO_2{\cdot}nH_2O$ nanoparticles with 2 nm in diameter functionalized 2-(4-amino-benzyl)malonic acid.

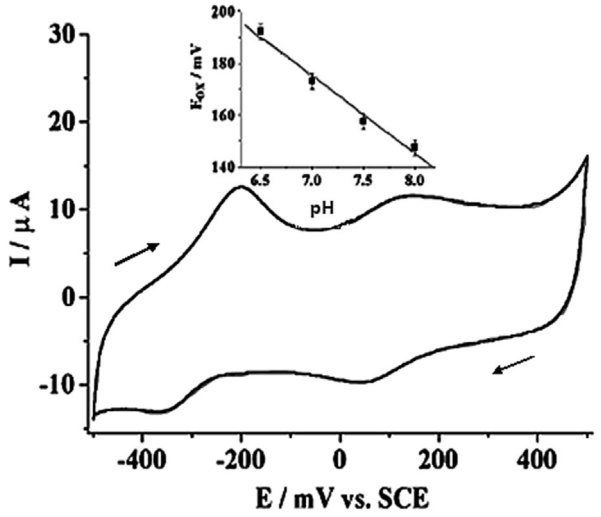

Fig. 4 – Cyclic voltammogram of electropolymerized $Ru(bpy)_2(bpyCONHAr)]^{+2}$ modified aniline and $IrO_2{\cdot}nH_2O$ nanoparticles functionalized with 2-(4-aminobenzyl) malonic acid film in the medium of 0.1 M phosphate buffer solution (pH = 7.4) at a scan rate of 100 mV s^{-1}. (Inset: Oxidation Peak potentials of crosslinked-oligoaniline formation depending on different pH values.)

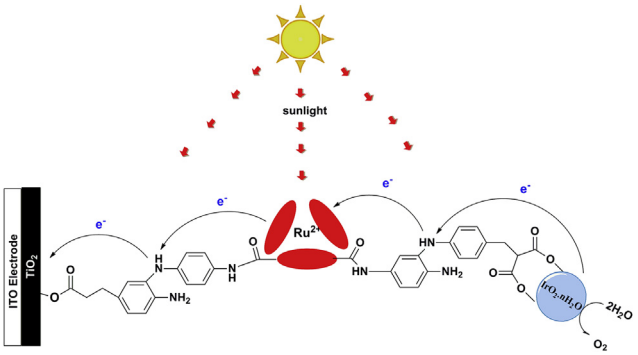

Fig. 5 – Schematic representation of working principle prepared photocurrent experiments in photoanode.

described experimental section. First, when $IrO_2{\cdot}nH_2O$ nanostructure modified ITO electrodes immersed in the water instead of pure ethanol under visible light, photocurrent wasn't observed to occur in any way. This experiment shows that the system is only sensitive to water and photocurrent occurs with electron transfer formed by water oxidation. Also, the system didn't create photocurrent, when ITO electrode modified with $TiO_2/[Ru(bpy)_2(bpyCONHAr)]^{+2}$ without $IrO_2{\cdot}nH_2O$ nanostructure attached via electropolymerization over TiO_2 film. It was sinked into phosphate buffer solution (pH = 7.4) in a visible light region. These three control experiments have shown that water, $[Ru(bpy)_2(bpyCONHArNH_2)]^{+2}$ dye and $IrO_2{\cdot}nH_2O$ nanoparticles are needed in order to create photocurrent. If the cause of photocurrent transition in the molecular level for this was asked to investigate, it can be expressed as follows. When the light was sent to $Ru(bpy)_2(bpyCONHArNH_2)]^{+2}$ dye in the water, an electron in the valence band of $Ru(bpy)_2(bpyCONHArNH_2)]^{+2}$ dye will jump to its excitation band and will continue to jump from there to the electrode. An electron gap in the valence band of $Ru(bpy)_2(bpyCONHArNH_2)]^{+2}$ dye will be filled by electrons emerged when the nanoparticles of $IrO_2{\cdot}nH_2O$ oxidize water. Because these incidents occur continuously, it generates a photocurrent. The mission of TiO_2 is to accelerate the transfer of electrons from system to the electrode (Fig. 5).

Fabrication of cathode electrode for solar cell

Synthesis and characterization of P (SNS-NH_2) and platinum nanoparticles functionalized with the mercaptoaniline (Fig. 6)
Platinum nanoparticles functionalized with the mercaptoaniline were characterized with TEM and SEM analysis. The size of Pt nanoparticles was found as 4–5 nm in diameter (Fig. 7).

P(SNS-NH_2) was electropolymerized on Au electrode in the proper solvent-electrolyte couple for electropolymerization. Working electrode potential was scanned from −0.5 V to 1.2 V vs Ag/AgCl repetitively. After the coated electrode was washed with ACN to remove the monomer and oligomeric species, Pt nanoparticles functionalized with mercaptoaniline was electropolymerized in phosphate buffer medium (pH = 7.4) by using CV method over P(SNS-NH_2) on gold electrode in the same potential window where SNS-NH_2 monomer was polymerized. In order to characterize composite synthesized, the film obtained was characterized in the medium of phosphate buffer solution (0.1 M). As seen cyclic voltammetry in Fig. 8, a redox couple was proved at around 0.1 V to the formation of crosslinked oligoanilines in the electrode system when the cathode electrode of photoelectrochemical cell, which was Au electrode modified with P(SNS-NH_2)/Pt nanoparticles functionalized with the mercaptoaniline structure was scanned at between −0.5 V and 0.5 V at a scan rate of 100 mV s^{-1} (Fig. 8).

Optimization of photoanode electrode components (ITO/ $TiO_2/[Ru(bpy)_2(bpyCONHArNH_2)]^{+2}$ dye/$IrO_2{\cdot}nH_2O$ nanoparticles) of solar cell

For last control experiments, $[Ru(bpy)_2(bpyCONHArNH_2)]^{+2}$ dye and $IrO_2{\cdot}nH_2O$ nanoparticles were electropolymerized over ITO electrode coated TiO_2. After this electrode was dipped into water when the light was sent at 460 nm, a photocurrent value was found as 13.5 μA/cm^2. In this control experiments, ITO electrode modified $[Ru(bpy)_2(bpyCONHAr)]^{+2}$ dye/$IrO_2{\cdot}nH_2O$ nanoparticles, which was prepared in the concentration ratio of 1.5/1, on 5 μm TiO_2 film in thickness was electropolymerized with 80 cycles and forms a composite of $[Ru(bpy)_2(bpyCONHArNH_2)]^{+2}$ dye and $IrO_2{\cdot}nH_2O$ nanoparticles (Fig. 9).

It was observed that the molar concentration ratio of $[Ru(bpy)_2(bpyCONHArNH_2)]^{+2}$ dye/$IrO_2{\cdot}nH_2O$ nanoparticles to one to another affected the performance of the photoanode. When $[Ru(bpy)_2(bpyCONHArNH_2)]^{+2}$ dye concentration in $[Ru(bpy)_2(bpyCONHArNH_2)]^{+2}$ dye/$IrO_2{\cdot}nH_2O$ nanoparticles composite was higher, photoanode was more sensitive and

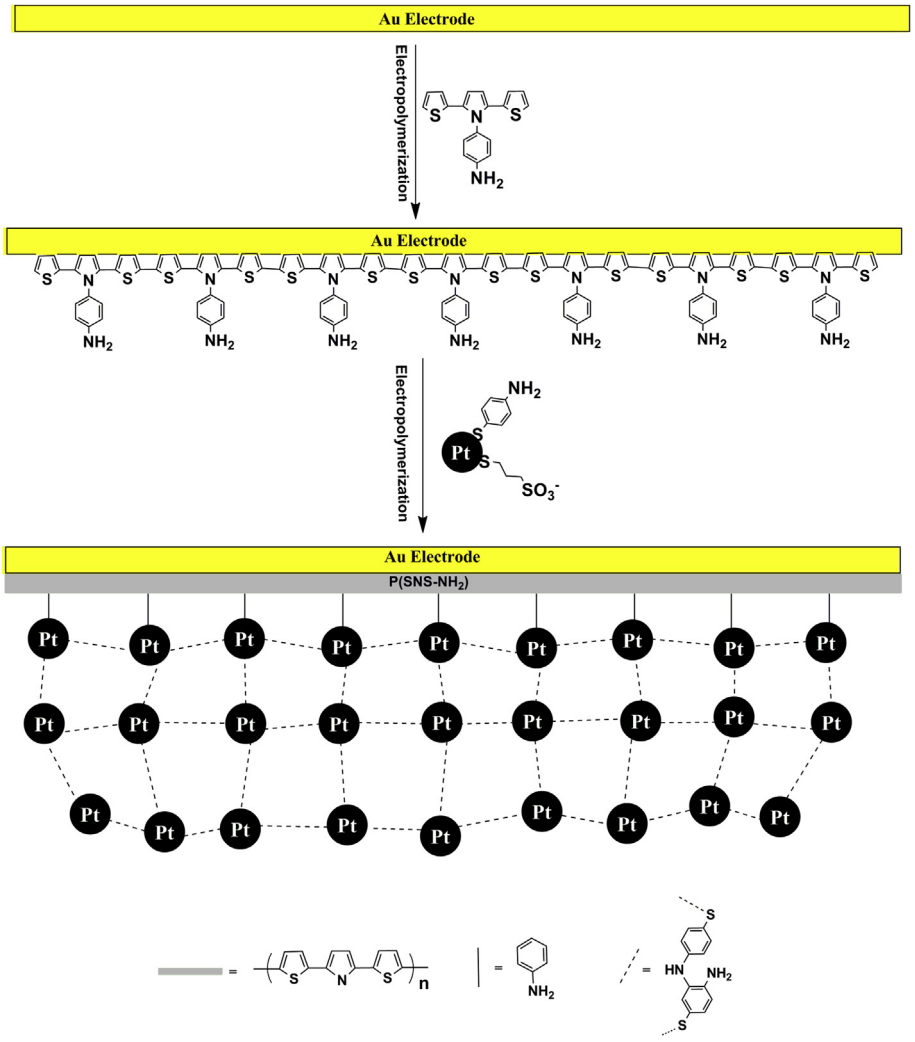

Fig. 6 – Schematic representation of the formation of crosslinked oligoaniline formations between P(SNS-NH_2) and Pt nanoparticles functionalized with the mercaptoaniline for cathode electrode in the photoelectrochemical cell.

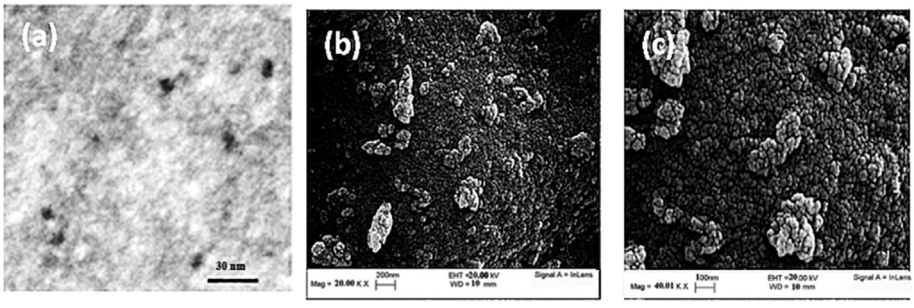

Fig. 7 – (a) TEM. (b) SEM images (200 nm) and (c) SEM images (100 nm) of platinum nano-particles functionalized with mercaptoaniline

better results for photoanode current formation were obtained.

On the other hand, one should realize that the covalent linkage of the $[Ru(bpy)_2(bpyCONHArNH_2)]^{+2}$ dye to $IrO_2 \cdot nH_2O$ nanoparticles perturbs the conductivity of the NPs (nanoparticles). That is, in the presence of high dye concentrations in the electropolymerization solution, the effective coverage of primary NPs linked to TiO_2 modified electrode is low, which insulates the particles towards further electropolymerization, and leads to a low total content of the dye in the resulting composite. The increase of the dye concentration in the solution to form composite prepared by electropolymerization reduces the number of nanoparticles connected to the electrode and gets lower the oxidation performance of the system

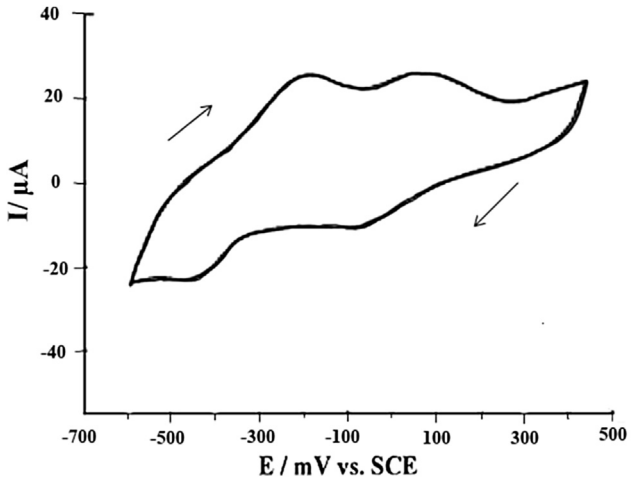

Fig. 8 – Cyclic voltammogram of electropolymerized P (SNS-NH_2)/Platinum Nano-particles functionalized with the mercaptoaniline structure in the medium of 0.1 M phosphate (pH = 7.4) solution at a scan rate of 100 mV s^{-1}.

and causes decreasing photoanode response [30]. In molar concentration optimization experiments, the optimum concentration molar ratio of $[Ru(bpy)_2(bpyCONHArNH_2)]^{+2}$ dye/$IrO_2{\cdot}nH_2O$ nanoparticles was found to be 2.1 (Fig. 10(a)).

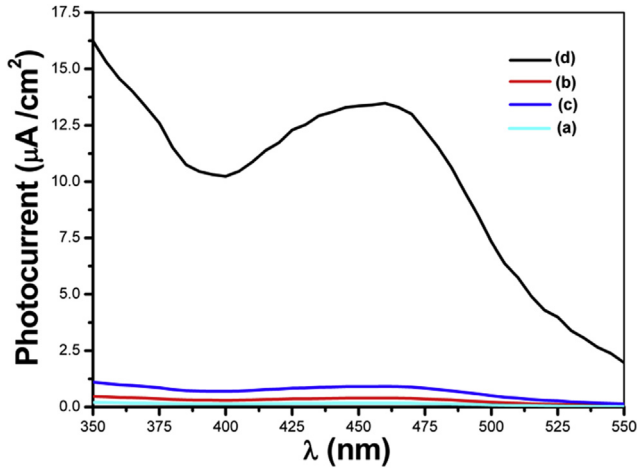

Fig. 9 – Photocurrent spectrums, showing the results of the formation on the result of the illuminated under visible light, when used a) ITO electrode modified with the structure of TiO_2/$[Ru(bpy)_2(bpyCONHArNH_2)]^{+2}$ dye/$IrO_2{\cdot}nH_2O$ nanoparticles in absolute ethanol, b) ITO electrode modified with the structure of TiO_2/$IrO_2{\cdot}nH_2O$ nanoparticles in 0.1 M phosphate buffer solution (pH 7.4), c) ITO electrode modified with the structure of TiO_2/$[Ru(bpy)_2(bpyCONHArNH_2)]^{+2}$ dye in 0.1 M phosphate buffer solution (pH 7.4), d) ITO electrode modified with the structure of TiO_2/$[Ru(bpy)_2(bpyCONHArNH_2)]^{+2}$ dye/$IrO_2{\cdot}nH_2O$ nanoparticles in 0.1 M phosphate buffer solution (pH = 7.4). 0 V (vs Ag/AgCl reference electrode) potential was applied in all spectra.

The number of cycles in the CV performed to form the composite is another optimization work. In this optimization study, $[Ru(bpy)_2(bpyCONHArNH_2)]^{+2}$ dye/$IrO_2{\cdot}nH_2O$ nanoparticles structure on TiO_2 film with 5 μm thickness is used in the ratio of 2/1. $[Ru(bpy)_2(bpyCONHArNH_2)]^{+2}$ dye/$IrO_2{\cdot}nH_2O$ nanoparticle composites were formed by electropolymerization in the numbers of 20, 40, 60, 80, 100 cycles. As the number of cycle increased for electropolymerization to create composite, the intensity of photocurrent received also rised. This situation continued up to 80 cycles. This increase in the number of amperometric response has been stopped until after 80 cycles. As the cause of photocurrent increase up to 80 cycles, an increase in the amount of gold that make up the composite nanoparticle composites with $IrO_2{\cdot}nH_2O$ nanoparticles can be considered.

Although the amount of nanoparticles in the composite occurred in 80 and 100 numbered cycles increases, photocurrent increase achieves saturation at one point and after that it causes very quickly growing confusion in the conductivity path as the number of cycles increase. It results in a decrease in conductivity and can be shown as a reduction in the rate of electron transfer [22]. It was decided to create a composite cycle count of 80 as the optimal number of cycles (Fig. 10(b)).

This optimization work on the ITO electrode 2.5; 5.0; 7.5; 10; 12.5; 15; 17.5 and 20 μm TiO_2 films in thick coated. $[Ru(bpy)_2(bpyCONHArNH_2)]^{+2}$ dye/$IrO_2{\cdot}nH_2O$ nanoparticles composite was formed with 80 cycles via CV in the ratio of 2/1 molar concentration over TiO_2 films in various thickness, and ITO electrodes modified with TiO_2/$[Ru(bpy)_2(bpyCONHArNH_2)]^{+2}$ dye/$IrO_2{\cdot}nH_2O$ nanoparticles. Photocurrent measurements were performed under ambient visible light in phosphate buffer (pH 7.4). Photocurrent was observed to increase up to the film thickness 12.5 μm. It was observed a decrease in the value of photocurrent received from the electrodes prepared using more than 12.5 μm. The reason is that 12 μm TiO_2 film in thick is the optimum thickness for the transfer of electrons in the TiO_2 film. The cause of this can be explained as follows. TiO_2 films prepared with a thickness of 15 μm and thicker than it are too thick to transfer electrons and this decreases photocurrent of the system (Fig. 10(c)).

UV light stability of the ITO electrode modified $[Ru(bpy)_2(bpyCONHArNH_2)]^{+2}$ dye/$IrO_2{\cdot}nH_2O$ nanoparticles was also investigated. ITO electrode modified $[Ru(bpy)_2(bpyCONHArNH_2)]^{+2}$ dye/$IrO_2{\cdot}nH_2O$ nanoparticles was exposed to UV light for 10; 20; 40; 60; 80, 100 h using a UV lamp (400 W and 110/220 V). After each exposure of the system to UV lamp, Clark type electrode system was used to understand how much oxygen it was produced when illuminated a certain time. 3-electrode system described beforehand was again used for this experiment. It was produced 3.12×10^{-9} mol/cm^2 oxygen gaseous by electrodes which were not exposed to UV-light illuminated at 460 nm for 20 min. Ones exposed to UV light for 10, and 15 h produced 3.09×10^{-9} mol/cm^2 and 3.02×10^{-9} mol/cm^2 respectively but after UV light exposure to system for more than 20 h, oxygen gas production began to fall dramatically. This case indicates that the TiO_2 film on the electrode illuminated for 20th hours is stable and works fully effective (Fig. 10(d)).

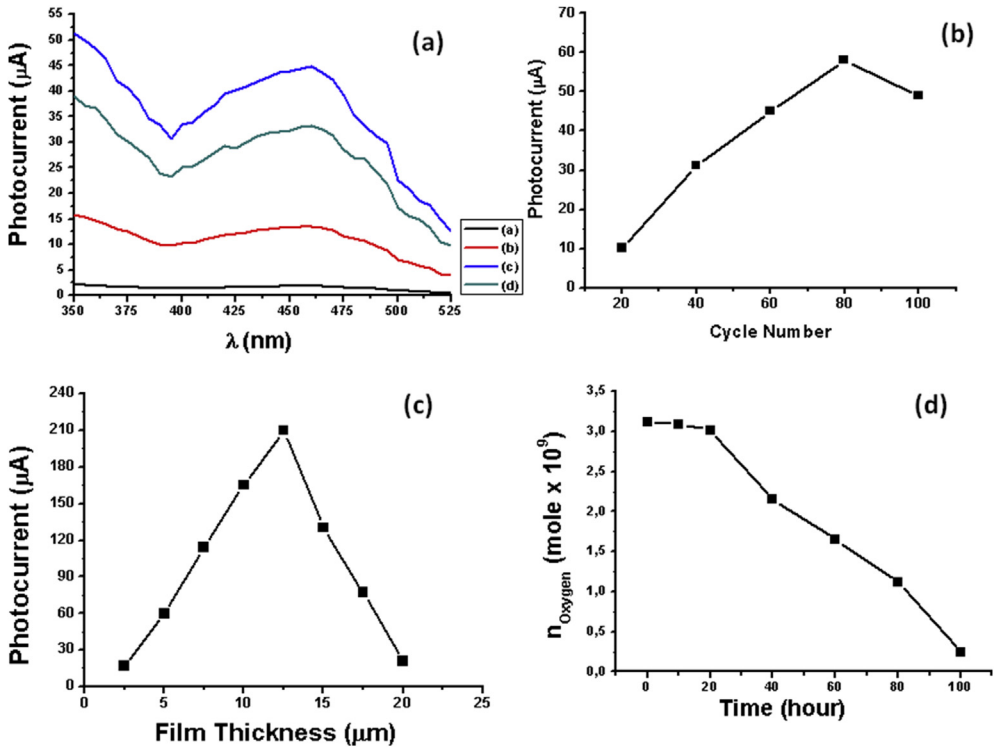

Fig. 10 – Optimization studies for photoanode of the system (a) the molar concentration ratio optimization of TiO_2/$[Ru(bpy)_2(bpyCONHArNH_2)]^{+2}$ dye/$IrO_2{\cdot}nH_2O$ nanoparticles a)1/1, b)1.5/1, c)2/1, d) 2.5/1. (b) CV number optimization for $Ru(bpy)_2(bpyCONHArNH_2)]^{+2}$ dye/$IrO_2{\cdot}nH_2O$ nanoparticles structure on TiO_2 film. (c) Film thickness optimization of TiO_2. (d) UV light stability of the ITO electrode modified $[Ru(bpy)_2(bpyCONHArNH_2)]^{+2}$ dye/$IrO_2{\cdot}nH_2O$ nanoparticles in the medium of 0.1 M buffer solution (pH = 7.4) when illuminated under visible light region of the spectrum. 0 V (vs Ag/AgCl reference electrode) potential was applied in all spectra.

Time-dependent production of oxygen gas for ITO electrode modified $[Ru(bpy)_2(bpyCONHArNH_2)]^{+2}$ dye/$IrO_2{\cdot}nH_2O$ nanoparticles by oxidizing water

The following graph was obtained using three electrode system containing ITO electrode modified TiO_2/$[Ru(bpy)_2(bpyCONHArNH_2)]^{+2}$ dye/$IrO_2{\cdot}nH_2O$ nanoparticle by using Clark-type electrode to understand how much oxygen was produced in the water system when ITO electrode modified TiO_2/$[Ru(bpy)_2(bpyCONHArNH_2)]^{+2}$ dye/$IrO_2{\cdot}nH_2O$ was illuminated for a certain period of time. After the system was illuminated for 20 and 25 min, the amount of oxygen produced by ITO electrodes modified TiO_2/$[Ru(bpy)_2(bpyCONHArNH_2)]^{+2}$ dye/$IrO_2{\cdot}nH_2O$ nanoparticle, were calculated as 3.12×10^{-9} mol/cm^2 and 3.15×10^{-9} mol/cm^2, respectively (Fig. 11). The oxygen evolution rate of this electrode was found approximately 0.74 μmol/min. Compared with the results of similar structures in this literature [31], the oxygen evolution rate is approximately 3–7 times faster than for $[Ru(bpy)_3]^{2+}$/succinate-IrO_2 (0.22 μmol/min), $[Ru(dcb)_2(bpy(CONHSA)_2]^{6-}$-$IrO_2$ (0.13 μmol/min) and $[Ru(dcb)_3]^{4-}$-IrO_2 (0.10 μmol/min), respectively. The remarkable enhancement can be ascribed the preventing back electron transfer as well as reducing recombination rate with incorporation of oligoaniline crosslinked bridging units into this device [32].

Another characterization study of ITO electrode modified $[Ru(bpy)_2(bpyCONHArNH_2)]^{+2}$ dye/$IrO_2{\cdot}nH_2O$ nanoparticles is on-off study of the system. It was illuminated at 460 nm for a certain time with a fixed light source and then illumination were finalized. After this procedure was repeated several

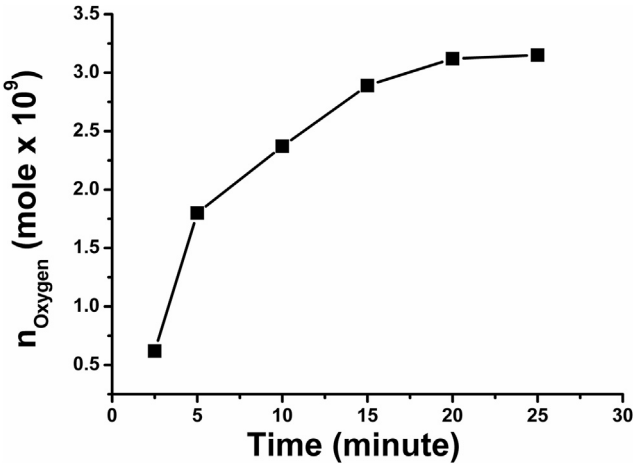

Fig. 11 – Time-dependent production of oxygen gas for ITO electrode modified $[Ru(bpy)_2(bpyCONHArNH_2)]^{+2}$ dye/$IrO_2{\cdot}nH_2O$ nanoparticles by oxidizing water.

times, a decrease in the amount of photocurrent obtained was observed because oxygen gas formed by the oxidation of water penetrates of the forward electron transfer rate forming photocurrent. In this study, It is aimed to remove the oxygen gas from the medium forming as a result of the illumination of the ITO electrode modified $[Ru(bpy)_2(bpyCONHArNH_2)]^{+2}$ dye/$IrO_2 \cdot nH_2O$ nanoparticles by of bilirubin oxidase enzyme (1.5 mg/mL) whose one of the substrates is oxygen in the electrolyte. After this addition, there was no decrease in the amount photocurrent obtained when the light source was switched off (on-off). This event is supported by our description in the photocurrent decrease. (Fig. 12(a) and (b)).

Optimization of cathode electrode components (Au/P(SNS-NH_2)/Pt nanoparticles) of solar cell

One of the most important features of Pt nanoparticles was to reduce H_2O_2 to water by electrocatalyzing. This study aims that Pt nanoparticles will reduce the protons resulting from the separation of water by oxidation to hydrogen gas. Optimization of the required surface for the correct electron transfer to be fastest from the electrode through Pt nanoparticles, reduction of H_2O_2 was utilized. From this knowledge, it is considered to be the same number of protons for the conversion of hydrogen gas during water splitting process (Fig. 13(a)).

The first characterization studies of P(SNS-NH_2)/Pt cathode electrode which will be a part of photochemical cell, are optimization studies related with the number of cycles for CV method in order to coat Pt nanoparticles with oligoanilines to P(SNS-NH_2) on gold electrodes. Pt nanoparticles were cross-linked oligoaniline to the electrode coated with conjugated polymer (P(SNS-NH_2)) electropolymerized with 40, 60, 80 and 100 cycles. In order to find the optimum number of cycles, the CV's of P(SNS-NH_2)/Pt nanoparticles electrodes in the range of 0.2 V and −0.6 V potential difference was obtained in the presence of 9 mM hydrogen peroxide.

The optimal number of cycles required for connecting Pt nanoparticles to the conductive polymer was found from the net current difference in the cyclic voltammogram when Pt nanoparticles reduced H_2O_2 to water. It was observed that current difference in the voltammogram also increased in order to create composite, when the number of electropolymerization cycle number was increased. As shown in (Fig. 13(b)), the current increase in the voltammogram continued to 80 cycles, and it decreased in the 100th cycle. It was thought that the reason for the current difference increase up to 80 cycles, which causes the increase oligoaniline composite with a binding amount of Pt nanoparticles, was an increase of Pt nanoparticles in the composite. Although the amount of the Pt nanoparticles in the composite increased, it was observed that the current difference decreased in the 100th cycle because Pt nanoparticles caused a commotion and sealed the ways of conductivity resulting in reduced conductivity and a reduction in the rate of electron transfer [22]. In this optimization experiment, the optimum cycle number was decided to be 80, to form composite oligoaniline bonds between Pt nanoparticles and P(SNS-NH_2) polymer.

Another optimization study is the work of finding the optimum number of cycles in the cyclic voltammetry. In the previous optimization study, the number of cycle to electropolymerize the monomer was chosen as 80. In this part, SNS-NH_2 monomer was electropolymerized with different cycle numbers (10, 40, 60, 80, 100 and 120) on the gold electrode. The above polymer films obtained through several cycles number connected to Pt nanoparticles (1 mg/mL) via electropolymerization by applying 80 cycles of cyclic voltammetry was used as the cathode in this study and P(SNS-NH_2)/Pt nanoparticles modified gold electrode was obtained. In 0.1 M phosphate buffer (pH 7.4), cyclic voltammograms were taken in the range of 0.2 V and −0.6 V potential difference using 9 mM H_2O_2. It was found that the highest current difference in cyclic voltammograms belonged to 100th cycle of P(SNS-NH_2). The current difference of the polymer obtained with 120 cycles was decreased through the electrode since the film was very thick for electron transfer and electron didn't not reach far enough to be described as electrodes (Fig. 13(c)).

Water splitting experiments under visible light: determination of H_2 via gas chromatography method

The anode and cathode electrodes to the potentiostat device were connected in series with a resistance of 1 kΩ. A multimeter was also used to measure the voltage across the resistor

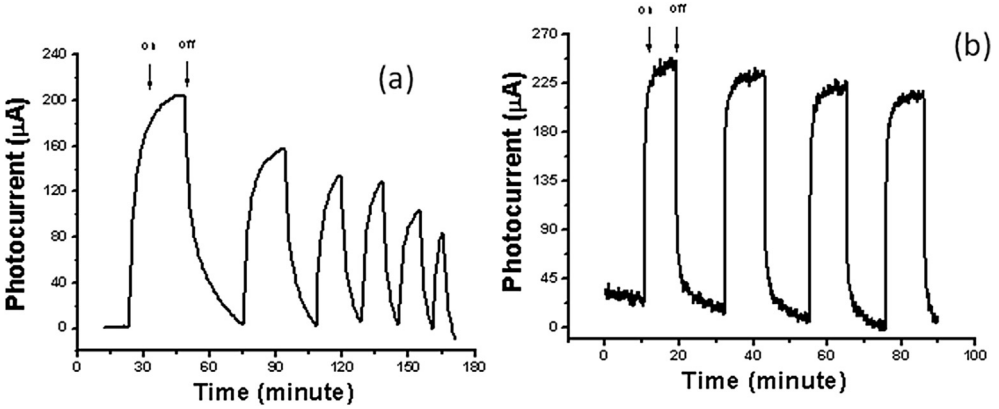

Fig. 12 – Displaying the on-off operation the photocurrent obtained (a) the effect of oxygen gas produced by the oxidation of water to the photocurrent obtained. (b) Indicating on–off operations of the oxygen gas produced by the oxidation of water removed by the help of bilirubin oxidase.

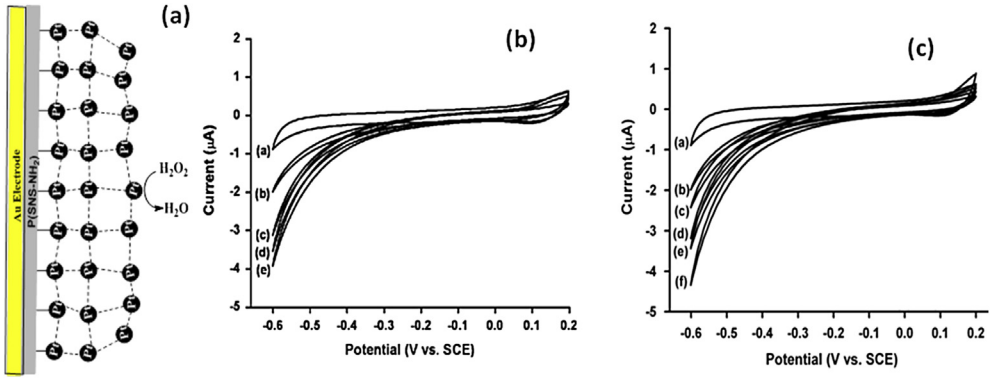

Fig. 13 – (a) The schematic representation of P (SNS-NH_2)/Pt nanoparticles modified gold electrodes in the reduction of hydrogen peroxide to water. (b) a) P (SNS-NH_2) coated gold electrode, b) 40, c) 60 d) 100, and e) 80 number of cycles with the Pt nanoparticles are obtained as a result of electropolymerization P (SNS-NH_2)/Pt nanoparticles of modified gold electrode in the presence of 9 mM H_2O_2. (c) a) 10, b) 40, c) 60, d) 80, e) 100 and f) 120 number of cycles polymerized SNS-NH_2 monomer on Pt nanoparticles of 80 cycles obtained as a result of electropolymerization P (SNS-NH_2)/Pt nanoparticles modified gold voltammogram alternating electrodes in the presence of 9 mM H_2O_2.

of resistance. 580 nm wavelength light was sent from the solar simulator to the established system were illuminated with 2.5; 5; 7.5; 10; 12.5; 15 and 20 min duration (Fig. S2 (a–e)). H_2 gas produced by the cathode of the system was determined by gas chromatography using the gas sample taken from the system via microsyringe. In the calculations, the system 1.25×10^{-8} mol hydrogen gas was produced in the system after illuminated with light at 580 nm for 20 min (Fig. 14). The quantum efficiencies for the generation of the photocurrents were determined by the electropolymerization of the $[Ru(bpy)_2(bpyCONHArNH_2)]^{+2}$ dye/and $IrO_2 \cdot nH_2O$ nanoparticles dye aggregated composites on transparent TiO_2 coated gold electrode [22]. These measurements provide the absolute values of the charge separation efficiencies, independent with respect to the content of photoactive $[Ru(bpy)_2(bpyCONHArNH_2)]^{+2}$ dye and the screening of the absorbance of the $[Ru(bpy)_2(bpyCONHArNH_2)]^{+2}$ dye nanoparticles by $IrO_2 \cdot nH_2O$ nanoparticles. We find that the quantum efficiency of light-to-electrical energy conversion corresponds to 3.5% for H_2 evolution and photocurrent generation.

Comparing different studies, we find that Poly(SNS-NH_2) functionalized platinum nanoparticles is a better catalyst and have much higher activity as photocatalysts for hydrogen evolution than only Pt nanoparticles at the same loading in the literature [33,34]. The significant increase in rate of hydrogen evolution are consistent with faster electron transfer between the 4-mercaptoaniline-substituted Pt nanoparticles and the Au metal when the Pt nanoparticles are capped by the P(4-(2,5-di(thiophen-2-yl)-1*H*-pyrrol-1-yl)benzamine) conducting polymer having good light harvesting in the visible region [31,35].

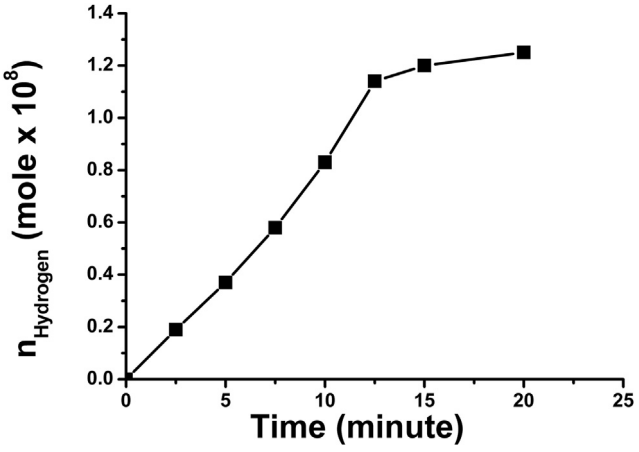

Fig. 14 – Hydrogen gas production depending on the time of solar cell.

Conclusions

In sum, a photoelectrochemical water splitting system which converts solar energy to chemical energy stored in hydrogen, knowing as a significant energy density fuel, was successfully constructed using visible light under constant applied voltage. For the (photo)anode site of the system, 2-(4-aminobenzyl) malonic acid-conjugated $IrO_2 \cdot nH_2O$ nanoparticles and $[Ru(bpy)_2(bpyCONHArNH_2)^{+2}]$ being a visible light absorbing dye arrayed via oligoaniline crosslinking onto TiO_2-modified ITO surfaces was performed to split H_2O into $4H^+$, O_2 and $4e^-$. For the (photo) cathode site of the system, an embedding gold electrode surfaces with both P(4-(2,5-di(thiophen-2-yl)-1*H*-pyrrol-1-yl)benzamine) conducting polymer and 4-mercaptoaniline-substituted Pt nanoparticles was employed to convert free $2H^+$ into H_2. The results reveal that our system significantly enhances not only the generation of photocurrent in visible light and the quantum yield but also production of O_2/H_2 recycle efficiency. Regarding this point, our system would be a good challenge to renewable photocurrent generation systems as well as this system will facilitate the rational

design of effective photo(anodes/cathodes) for solar-water splitting technology.

Acknowledgment

The authors would like to thank the European Union through the COST Action CM1104 "Reducible Oxide Chemistry, Structure and Functions" and the Scientific and Technological Research Council of Turkey (TUBITAK Grant Number 112T622) for the financial support of this work.

Appendix A. Supplementary data

Supplementary data related to this article can be found at http://dx.doi.org/10.1016/j.ijhydene.2016.04.249.

REFERENCES

[1] Ashokkumar M. An overview on semiconductor particulate systems for photoproduction of hydrogen. Int J Hydrogen Energy 1998;23:427–38.
[2] Ni M, Leung MKH, Leung DYC, Sumathy K. A review and recent developments in photocatalytic water-splitting using TiO_2 for hydrogen production. Renew Sustain Energy Rev 2007;11(3):401–25.
[3] Chen XB, Shen SH, Guo LJ, Mao SS. Semiconductor-based photocatalytic hydrogen generation. Chem Rev 2010;110(11):6503–70.
[4] Cargnello M, Diroll BT. Tailoring photocatalytic nanostructures for sustainable hydrogen production. Nanoscale 2014;6:97–105.
[5] McKone JR, Lewis NS, Gray HB. Will solar-driven watersplitting devices see the light of day? Chem Mater 2014;26(1):407–14.
[6] Dismukes GC. Splitting water. Science 2001;292:447–8.
[7] Nowotny J, Sorrell CC, Sheppard LR, Bak T. Solar-hydrogen: environmentally safe fuel for the future. Int J Hydrogen Energy 2005;30:521–44.
[8] Fujishima A, Honda K. Electrochemical photolysis of water at a semiconductor electrode. Nature 1972;238:37–8.
[9] Young KJ, Martini LA, Milot RL, Snoe III RC, Batista VS, Schmuttenmaer CA, et al. Light-driven water oxidation for solar fuels. Coord Chem Rev 2012;256(21–22):2503–20.
[10] Kudo A. Recent progress in the development of visible light-driven powdered photocatalysts for water splitting. Int J Hydrogen Energy 2007;32:2673–8.
[11] Minggu LJ, Daud WRW, Kassim MB. An overview of photocells and photoreactors for photoelectrochemical water splitting. Int J Hydrogen Energy 2010;35:5233–44.
[12] Veluru JB, Manippady KK, Rajendiren M, Mya KM, Rayavarapu PR, Appukuttan SN, et al. Photocatalytic hydrogen generation by splitting of water from electrospun hybrid nanostructures. Int J Hydrogen Energy 2013;38:4324–33.
[13] Joya KS, Joya YF, de Groot H. Ni-based electrocatalyst for water oxidation. Angew Chem Int Ed 2013;52:2–14.
[14] Joya DKS, Vallés-Pardo JL, Joya DF, Eisenmayer T, Thomas B, Buda DF, et al. Molecular catalytic assemblies for electrodriven water splitting. ChemPlusChem 2013;78(1):35–47.
[15] Youngblood WJ, Lee SHA, Maeda K, Mallouk TE. Visible light water splitting using dye-sensitized oxide semiconductors. Acc Chem Res 2009;42(12):1966–73.
[16] Licht S, Wang B, Mukerji S, Soga T, Umeno M, Tributsch H. Over 18% solar energy conversion to generation of hydrogen fuel; theory and experiment for efficient solar water splitting. Int J Hydrogen Energy 2001;26:653–9.
[17] Duan L, Tong L, Xua Y, Sun L. Visible light-driven water oxidation-from molecular catalysts to photoelectrochemical cells. Energy Environ Sci 2011;4(9):3296–313.
[18] Tan Y, Zhang S, Shi R, Wang W, Liang K. Visible light active $Ce/Ce_2O/CeO_2/TiO_2$ nanotube arrays for efficient hydrogen production by photoelectrochemical water splitting. Int J Hydrogen Energy 2016;41:5437–44.
[19] Kao LC, Huang Y, Banares MA, Liou SYH. Uniform deposition of coupled CdS and CdSe quantum dots on ZnO nanorod arrays as electrodes for photoelectrochemical solar water splitting. Int J Hydrogen Energy 2015;40:1388–93.
[20] Youngblood WJ, S-H Anna Lee, Kobayashi Y, Hernandez-Pagan EA, Hoertz PG, Moore TA, et al. Photoassisted overall watersplittinginavisible light-absorbing dye-sensitized photoelectrochemical cell. J Am Chem Soc 2009;131(3):926–7.
[21] Ismail AA, Bahnemann DW. Photochemical splitting of water for hydrogen production by photocatalysis: a review. Sol Energy Mater Sol Cells 2014;128:85–101.
[22] Yildiz HB, Tel-Vered R, Willner I. Solar cells with enhanced photocurrent efficiencies using oligoaniline-crosslinked Au/CdS nanoparticles arrays on electrodes. Adv Funct Mater 2008;18(21):3497–505.
[23] Karaman M, Sarıpek F, Köysüren O, Yildiz HB. Template assisted synthesis of photocatalytic titanium dioxide nanotubes by hot filament chemical vapor deposition method. Appl Surf Sci 2013;283:993–8.
[24] Valenty SJ, Gaines GLJ. Preparation and properties of monolayer films of surfactant ester derivatives of tris(2,2′-bipyridine)ruthenium(II)2+. J Am Chem Soc 1977;99(4):1285–7.
[25] Oki AR, Morgan RJ. An efficient preparation of 4,4′-dicarboxy-2,2′-bipyridine. Synth Commun 1995;25(24):4093–7.
[26] Rosenthal J, Nepomnyashchii AB, Kozhukh J, Bard AJ, Lippard SJ. Synthesis, photophysics, electrochemistry, and electrogenerated chemiluminescence of a homologous set of BODIPY-appended bipyridine derivatives. J Phys Chem C 2011;115(36):17993–8001.
[27] Zhang S, Cheng K, Wang X, Yin H. Selection, synthesis, and anti-inflammatory evaluation of the arylidene malonate derivatives as TLR4 signaling inhibitors. Bioorg Med Chem 2012;20(20):6073–9.
[28] Sayin S, Azak H, Yildiz HB, Camurlu P, Akkus GU, Toppare L, et al. Supramolecular assembly with enhanced photocurrents using semiconductor CdS nanoparticle-adorned Au electrode systems. Phys Chem Chem Phys 2015;17(30):19911–8.
[29] Yildiz E, Camurlu P, Tanyeli C, Akhmedov I, Toppare L. A soluble and multichromic conducting polythiophene derivative. J Electroanal Chem 2008;612(2):247–56.
[30] Yehezkeli O, Yan YM, Baravik I, Tel-Vered R, Willner I. Integrated oligoaniline-cross-linked composites of Au nanoparticles/glucose oxidase electrodes: a generic paradigm for electrically contacted enzyme systems. Chem Eur J 2009;15(11):2674–9.
[31] Hoertz PG, Kim YI, Youngblood WJ, Mallouk TE. Bidentate dicarboxylate capping groups and photosensitizers control the size of IrO_2 nanoparticle catalysts for water oxidation. J Phys Chem B 2007;111:6945–56.
[32] Morris ND, Suzuki M, Mallouk TE. Kinetics of electron transfer and oxygen evolution in the reaction of

$[Ru(bpy)_3]^{3+}$ with colloidal iridium oxide. J Phys Chem A 2004;108:9115–9.

[33] Hata H, Kobayashi Y, Bojan V, Youngblood WJ, Mallouk TE. Direct deposition of trivalent rhodium hydroxide nanoparticles onto a semiconducting layered calcium niobate for photocatalytic hydrogen evolution. Nano Lett 2008;8:794–9.

[34] Zhao Y, Swierk JR, Megiatto JD, Sherman Jr B, Youngblood WJ, Qin DD, et al. Improving the efficiency of water splitting in dye-sensitized solar cells by using a biomimetic electron transfer mediator. PNAS 2012;109:15612–6.

[35] Min S, Lu G. Dye-cosensitized graphene/Pt photocatalyst for high efficient visible light hydrogen evolution. Int J Hydrogen Energy 2012;37:10564–74.